中国科学: 物理学 力学 天文学 2025 年 第 55 卷 第 8 期: 286109
SCIENTIA SINICA Physica, Mechanica & Astronomica physcn.scichina.com
《中国科学》杂志社 SCIENCE CHINA PRESS
评 述 非晶态材料物理性能研究专辑

非晶态合金在催化领域的应用

吴用, 余鹏*

重庆师范大学物理与电子工程学院, 重庆 401331
*联系人, E-mail: pengyu@cqnu.edu.cn

收稿日期: 2024-09-25; 接受日期: 2024-12-20; 网络出版日期: 2025-03-10
国家自然科学基金(编号: 52371148)和重庆市自然科学基金创新发展联合基金(编号: CSTB2023NSCQ-LZX0138)资助项目

摘要 非晶态合金具有长程无序、短程有序的独特原子结构, 表现出一系列优异的力学、物理和化学性能. 近年来, 非晶态合金在催化领域的研究和应用受到了广泛关注. 与晶态结构相比, 非晶态结构具有不饱和位点多、潜在的吸附容量更大、耐腐蚀性好等优点. 无晶格、晶界和位错的限制使得其组分和电子结构具有更大的调控范围, 有利于最大程度提升合金的催化活性. 本文简要综述了非晶态合金催化剂的发展历程、结构优势以及在催化领域的应用潜力, 同时总结了其面临的挑战和应用前景.

关键词 非晶态合金, 催化剂, 性能优势, 应用前景

PACS: 61.43.Er, 71.55.Jv, 78.55.Qr, 82.47.-a, 84.60.-h

1 非晶态合金催化剂的发展历程

非晶态合金的研究始于20世纪[1], 1950年Brenner等人[2]采用电沉积法成功制备了Ni-P非晶态合金, 随后Ni-P非晶态合金镀层被广泛应用于金属表面的防护涂层, 这标志着非晶态合金的首次工业应用. 1959年, Cohen和Turnbull[3]提出了非晶态合金的形成理论, 为非晶态合金及其物理特性的研究奠定了基础. 1960年, Klement Jun.等人[4]通过熔体淬火技术制备了二元Au-Si非晶态合金, 标志着非晶态合金研究的新纪元. 自1960年以来, 非晶态合金的种类不断增加, 展现出多种特性[5]. 与晶态合金相比, 非晶态合金不仅具有金属特性, 还展现出许多与非晶态结构相关的独特性质, 成为理想的结构功能材料[6–8].

非晶态合金作为新型催化材料的研究始于1980年. Smith等人[9]在第七届国际催化会议上报道了关于非晶态合金作为催化剂的工作, 促进了非晶态合金在催化领域的迅速发展[10]. 1986年, van Wonterghem等人[11]使用化学还原法制备了超微非晶态合金粒子, 将“超微粒子”与“非晶态”两个概念结合在一起, 进一步推动了非晶态合金在催化领域的发展(图1)[12–21]. 20世纪80年代中期, 在闵恩泽的带领下, 中国石油化工股份有限公司石油化工科学研究院联合中石化生产企业和相关高校, 开始进行非晶态合金和磁稳定床反应工程技术的基础研究. 通过催化材料和反应工程的创新集成, 实现了跨越式发展, 并取得了重大经济和社会效益. 历经20年研发的“非晶态合金催化剂和磁稳定床反应工艺的创新与集成”项目, 荣获2005年国家技术发明

引用格式: 吴用, 余鹏. 非晶态合金在催化领域的应用. 中国科学: 物理学 力学 天文学, 2025, 55: 286109
Wu Y, Yu P. Application of amorphous alloys in catalysis (in Chinese). Sci Sin-Phys Mech Astron, 2025, 55: 286109, doi: 10.1360/SSPMA-2024-0410

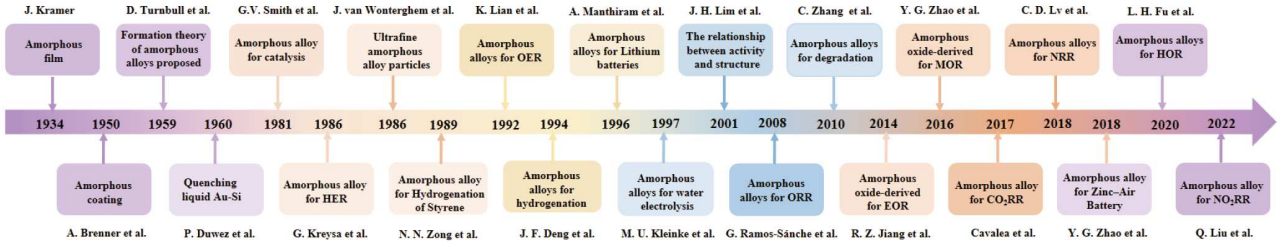

图 1　(网络版彩图)非晶态合金在催化领域的发展历程
Figure 1　(Color online) The development of amorphous alloy in the catalysis fields.

一等奖和2007年国家最高科学技术奖.

近年来，非晶态合金催化剂在催化领域受到越来越多的关注，在还原反应催化(包括析氢反应(HER)和氧还原反应(ORR)等)、氧化反应催化(包括析氧反应(OER)、醇氧化反应(AOR)和尿素氧化反应(UOR)等)以及污水处理等方面均取得了阶段性的重要进展. 本文简要综述了非晶态合金催化剂在催化领域的应用，为设计高活性、高稳定性的非晶态合金催化剂提供参考.

2　非晶态合金催化剂的结构优势

与稳定的晶态结构相比，非晶态合金被认为是亚稳的过渡中间态[22,23]. 它们类似液体的无序原子排列，使非晶态合金看起来像是“冻结”的无序固体(图2)[7,24]. 长期以来，人们主要关注各种晶体材料的结构和性能，对非晶态合金的结构特征和性能研究仍处于探索阶段，没有形成固定的研究范式. 因此，尽管对非晶态合金的研究已有近百年，但目前对非晶态合金催化剂的研究仍处于初步探索阶段[25]. 随着研究技术的蓬勃发展和材料制备方法的不断改进，特别是先进表征技术和理论计算方法的应用，各种新型非晶态合金催化剂不断被开发出来[26,27].

非晶态合金作为新型高效催化剂，在能源储存和转换领域中具有广泛的应用前景. 与晶态材料相比，非晶态合金具有如下优势：(1) 非晶态合金催化剂可以在很宽的范围内调整其成分结构，有利于电子结构的有效调节，从而获得合适的催化活性中心. (2) 非晶态合金催化剂具有各向同性，不存在晶界、堆垛层错和偏析等缺陷，且活性位点均匀. 由于腐蚀往往从晶界开始，因此非晶态合金催化剂相较于晶态催化剂具有优异的抗腐蚀性能. (3) 非晶态合金的制备方法灵活且多样，可根据需求选择制备方式，从而降低生产成本. (4) 非晶态合金具有较高的表面能及大量不饱和位点. 表面金属位点在大多数情况下充满悬空键，使一些化学反应物及中间产物能够适当地吸附在特定位点上，并在适当的条件下发生反应. (5) 非晶态合金具有亚稳态结构，在极端物理或化学条件下易发生表面重构，从惰性物种转变为活性物种. 因此，非晶态合金催化剂独特的结构优势使其成为一种具有重大应用前景的催化剂材料.

3　非晶态合金催化剂的应用

为了实现碳中和和碳达峰的发展目标，减少传统化石能源的使用是关键. 由于催化反应既能生产又能储存可持续的清洁能源，所以开发高效催化剂用于能源催化反应是一个行之有效的途径[28,29]. 尽管不同催化反应过程产生的可持续能源依赖不同的反应机理，但其实现及最终商业化必须依赖于高性能催化剂的开发. 非晶态合金作为催化剂具有天然的优势，在催化领域，如还原反应催化(包括析氢反应(HER)和氧还原反应(ORR)等)、氧化反应催化(包括析氧反应(OER)、醇氧化反应(AOR)和尿素氧化反应(UOR)等)和污水处理等方面具有巨大的应用潜力.

3.1　还原反应

3.1.1　析氢反应(HER)

氢能是一种来源丰富、绿色低碳和应用广泛的二次能源，正逐步成为全球能源转型发展的重要载体之一[30]，但氢能的发展仍面临诸多问题和挑战. 目前，主要是通过化石能源和工业副产制氢等方法制氢，而采用可再生能源制氢的规模仍然较小，并且用可再生能源制造的氢气才是我们所需要的“绿氢”[31]. 在现有的

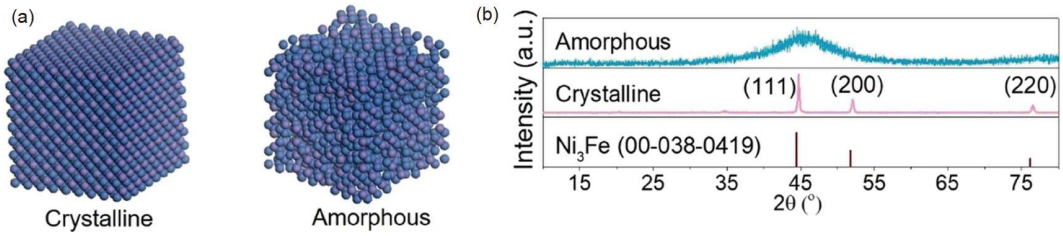

图 2　(网络版彩图) Ni_3Fe晶体和Ni_3Fe非晶态合金的原子模型(a)和XRD图谱(b)[24]
Figure 2　(Color online) Atomic model (a) and XRD patterns (b) of crystalline and amorphous Ni_3Fe alloys [24].

制氢技术中，电解水制氢是制备“绿氢”最为广泛使用且行之有效的方法[32]. 在传统的电解槽中，反应是在适当的电解液中进行的, 通常使用硫酸(H_2SO_4)和氢氧化钾(KOH)作为电解液, 分别提供酸性和碱性条件. 析氢反应(HER)作为电解水过程中至关重要的半反应, 在可持续能源转换和储存领域发挥着举足轻重的作用[33]. 该反应涉及两电子转移过程，形成中间氢(H*), 并且受电解液pH值的影响较大[34].

HER的发生需要引入能够降低活化能、加快反应动力学的催化剂. 在研究的非晶态合金催化剂中, 通过电弧熔炼和熔融甩带技术制备的$Fe_{40}Co_{40}P_{13}C_7$[35], $Pd_{40}Cu_{30}Ni_{10}P_{20}$[36]和$Ir_{25}Ni_{33}Ta_{42}$[37]等非晶态合金条带可以作为HER催化剂. 对于传统的电极而言, 活性位点位于电极外表面，几何面积约等于电化学活性面积(ECSA). 因此，对于一些纳米材料或3D材料电极，尤其是一些多孔电极, 其比表面积很大, 会大幅度地增加ECSA, 提升电催化性能[38]. 由于非晶条带的表面常常比较光滑，因此增加其比表面积和反应接触位点从而改善电催化活性是至关重要的. 2021年，Jia等人[39]设计了PdPtCuNiP高熵非晶态合金条带(图3(a))，脱合金后直接用作HER电极，无论是在碱性还是酸性条件下均显示出优异的HER活性(图3(b)和(c)). 电流密度为10 mA cm^{-2}时，在1.0 mol L^{-1} KOH和0.5 mol L^{-1} H_2SO_4溶液中的过电位(η)分别为32和62 mV，其性能与商业催化剂(Pt/C)媲美. 在酸性和碱性电解液中的稳定性分别为90和100 h，且元素浸出和结构劣化几乎可以忽略不计, 这表明其具有巨大的商业潜力. 密度泛函理论(DFT)计算和实验表明(图3(d)–(g)), 在脱合金过程中生成的纳米晶具有轻微的晶格畸变，导致d带中心(E_d)向费米能级(E_F)偏移较大. 这是由Pt-Pd亚晶格中的P原子间隙固溶引起的, 这种固溶现象改善了Pt周围的电子结构，优化了氢中间体的吸附/脱附，从而提升了合金的HER性能. 2022年，Tian等人[40]对非晶$Ti_{37}Cu_{60}Ru_3$合金进行脱合金处理，制备了一种独立的纳米结构HER催化剂，研究了在TiCu合金中进行脱合金和添加Ru对微观结构在碱性条件下HER性能的影响. 在$Ti_{40}Cu_{60}$中添加3 at.%的Ru会降低过电位，当电流密度达到10 mA cm^{-2}时, 脱合金样品的过电位和Tafel斜率分别为35 mV和34 mV dec^{-1}. 电催化性能的改善归因于纳米结构的形成和催化剂电子结构的改变. DFT计算结果表明, Ru降低了电解水的吉布斯自由能. Chu等人[36]通过高压扭转(HPT)处理的$Pd_{40}Cu_{30}Ni_{10}P_{20}$非晶态合金，无论在酸性还是碱性电解液中都表现出优异的HER性能，而且不会引起明显的结构变化. 严重的塑性变形显著增加了非晶基体中流动单元的密度, 同时也增加了非晶态合金条带的褶皱, 进而增大了其ECSA. 经HPT处理的非晶态合金在0.5 mol L^{-1} H_2SO_4和1 mol L^{-1} KOH的电解液中，电流密度达到10 mA cm^{-2}时的过电位分别为76和209 mV，低于相同条件下熔融甩带的非晶态合金的179和379 mV. 表1[41–63]是近几年部分非晶态合金催化剂用于HER的汇总.

3.1.2　氧还原反应(ORR)

在过去的几十年中，阴极氧还原反应(ORR)产生过氧化氢(2e⁻ H_2O_2)引起了人们的极大兴趣, 而在电池能量转换过程中也会涉及四电子氧还原反应(4e⁻ ORR)[64]. ORR的反应过程复杂, 包括多个反应路径和中间产物. 反应路径可以简单地分为四电子路径和两电子路径，反应路径与电解液的酸碱性有关[65]. 当O_2分子吸附在反应活性位点时直接经历2e⁻ ORR过程, 生成的产物为H_2O_2. 然而，在碱性条件下的ORR途径更倾向于4e⁻的还原过程，最后转化成H_2O. 由于4e⁻ ORR途径的输出电压和能量转换效率高于2e⁻ ORR途

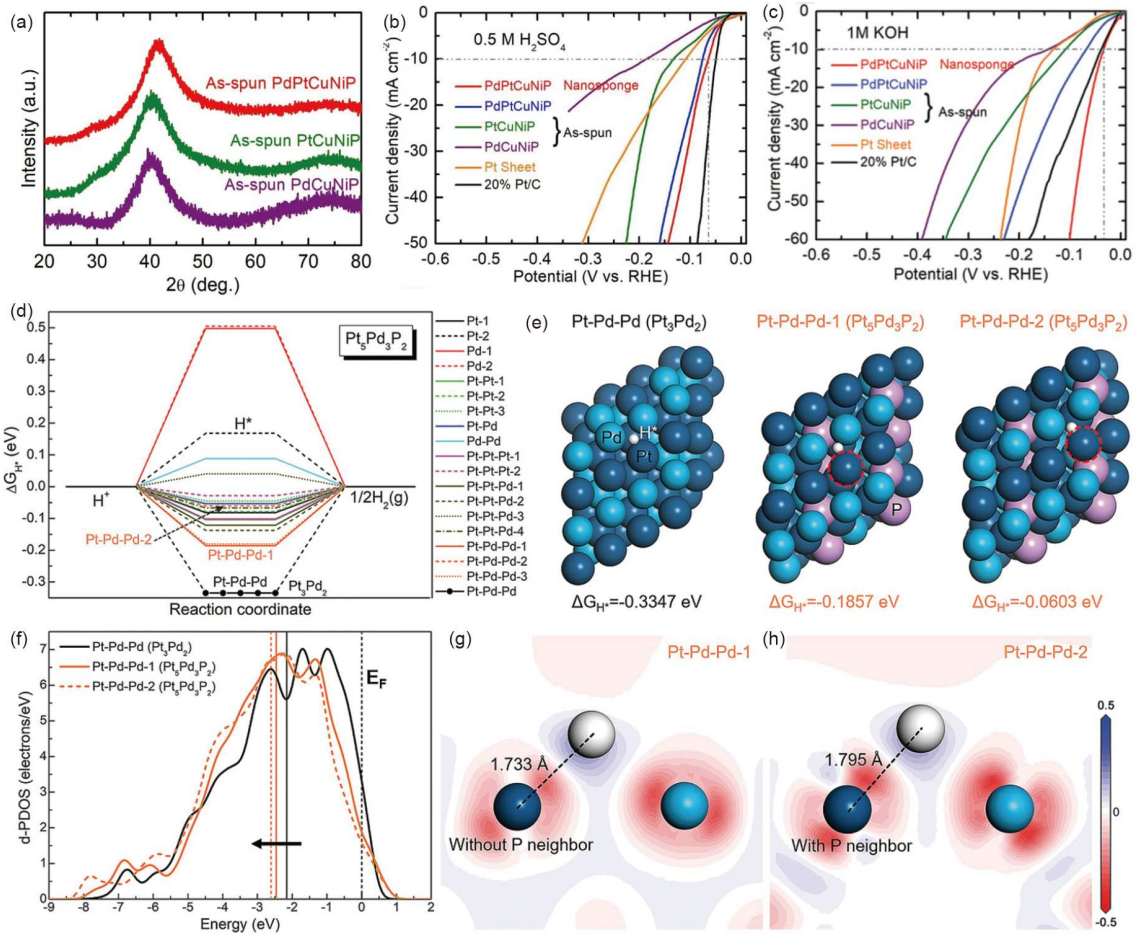

图 3　(网络版彩图) (a) XRD图谱; (b), (c) 在0.5 mol L^{-1} H_2SO_4 (b)和1 mol L^{-1} KOH (c)溶液中的线性扫描伏安(LSV)极化曲线; (d) $Pt_5Pd_3P_2$的吉布斯自由能曲线; (e) Pt_3Pd_2和$Pt_5Pd_3P_2$的Pt-Pd-Pd位点吸附H*的局部环境及相应的吉布斯自由能(ΔG_{H*})值; (f) Pt-Pd-Pd位点在不同环境在的d-PDOS和相应的d带中心(E_d); (g), (h) 在无P (g)和有P (h)的$Pt_5Pd_3P_2$表面上, H*吸附在Pt-Pd-Pd第一邻位配位位点后的电荷密度差分的DFT结果[39]

Figure 3　(Color online) (a) XRD patterns; (b), (c) polarization curves of LSV in 0.5 mol L^{-1} H_2SO_4 (b) and 1 mol L^{-1} KOH (c) solutions; (d) Gibbs free energy curve of $Pt_5Pd_3P_2$ surface; (e) the local environment of H* adsorbed at Pt-Pd-Pd sites of Pt_3Pd_2 and $Pt_5Pd_3P_2$ and the corresponding Gibbs free energy (ΔG_{H*}) values; (f) the d-PDOS results and the corresponding d-band center (E_d) for the Pt-Pd-Pd sites with different neighboring environments; (g), (h) DFT results of electron density differences after H* adsorption on Pt-Pd-Pd sites at the $Pt_5Pd_3P_2$ surface without (g) and with (h) first neighboring coordination of P [39].

径, 因此4e⁻ ORR过程得到了广泛的认可. 由于ORR的动力学过程缓慢, 通常需要更高的过电位才能获得实际电流密度[66], 导致实际电化学能量转换效率较低. 为了提高反应速率, 需要设计高效的催化剂, 以降低中间体之间过渡态的最大势垒.

在探索2e⁻ ORR催化剂时, 非晶态合金催化剂受到了研究者们的关注. 2022年, Wu等人[67]研究发现在0.2–0.6 V/RHE (可逆氢电极)的电位范围内, NiB_2非晶态合金催化剂对H_2O_2的选择性超过93%, 在0.4 V/RHE可达99%, 可以在12 h内保持优异的活性, 衰减可以忽略不计(图4(a)–(c)), 性能超过了之前报道的先进催化剂. 这种非晶态合金催化剂同时具有低成本、高活性、高选择性和稳定性的优点, 有效解决了2e⁻ ORR稳定性不足的问题.

除此之外, 在探索4e⁻ ORR催化剂时, 研究者们也发现了非晶态合金催化剂的优越性. 2023年, Fu等人[68]通过新型激光蒸发惰性气体冷凝法, 合成了一种具有球形形态的、新颖的$Pd_{40}Ni_{40}P_{20}$拓扑无序金属玻璃纳米颗粒(MGNP). 通过结构分析揭示了Pd-Ni-P MGNP团簇连接成中程序(MRO)时从两个原子模式转

表 1　非晶态合金的HER催化性能

Table 1　HER catalytic performance of amorphous alloys

催化剂	电解液	过电位	稳定性测试	文献
RhRuPtPdIr	0.5 mol L^{-1} H_2SO_4 1.0 mol L^{-1} PBS 1.0 mol L^{-1} KOH	η_{10} = 13 mV η_{10} = 77 mV η_{10} = 65 mV	12 h@−100 mA cm^{-2}	[41]
$Fe_{67}Co_{10}Ni_{10}Zr_{10}Pt_3$	1.0 mol L^{-1} KOH	η_{10} = 19 mV	250 h@−500 mA cm^{-2}	[42]
NiZrPt	1.0 mol L^{-1} KOH	η_{10} = 15 mV	100 h@−10 mA cm^{-2}	[43]
$Cu_{50}W_{50}$	1.0 mol L^{-1} KOH	η_{10} = 65 mV	200 h@−100 mA cm^{-2}	[44]
$Fe_{88.46}P_{9.42}$	1.0 mol L^{-1} KOH	η_{10} = 436 mV	207 h@−10 mA cm^{-2}	[45]
Co-P-B	1.0 mol L^{-1} KOH	η_{10} = 270 mV	10000 CV	[46]
CoP	1.0 mol L^{-1} KOH	η_{10} = 63 mV	2000 CV	[47]
a-CoPSe	1.0 mol L^{-1} KOH	η_{100} = 212 mV	1000 CV	[48]
FeCoCrMoCBY	0.5 mol L^{-1} H_2SO_4	η_{100} = 178 mV	120 h@−50 mA cm^{-2}	[49]
PdPtCuNiP	0.5 mol L^{-1} H_2SO_4	η_{10} = 35.4 mV	6 h@−1.25 V/RHE	[50]
$Pt_{25}Pd_{25}Ni_{25}P_{25}$	1.0 mol L^{-1} KOH	η_{10} = 19.8 mV	20 h@−60 mA cm^{-2}	[51]
$(FeCoNiB_{0.75})_{97}Pt_3$	1.0 mol L^{-1} KOH	η_{10} = 27 mV	48 h@−20 mA cm^{-2}	[52]
$Fe_{73.5}Si_{13.5}B_9Cu_1Nb_3$	1.0 mol L^{-1} KOH	η_{10} = 174 mV	40 h@CV	[53]
FeCoNiAlP	1.0 mol L^{-1} KOH	η_{10} = 134 mV	24 h@−1.34 V/RHE	[54]
FeNiCoMoP	1.0 mol L^{-1} KOH	η_{10} = 146 mV	24 h@−10 mA cm^{-2}	[55]
FeMoPC	0.5 mol L^{-1} H_2SO_4	η_{10} = 96 mV	16 h@−10 mA cm^{-2}	[56]
$Cu_{60}Ti_{37}Mo_3$	1.0 mol L^{-1} KOH	η_{10} = 220 mV	20 h@220 mV	[57]
$Ni_{69}P_{31}$	0.5 mol L^{-1} H_2SO_4	η_{10} = 275 mV	1600 CV	[58]
NiMo	KOH (PH = 10)	η_{10} = 63.9 mV	100 h@−10 mA cm^{-2}	[59]
Ni-Ce-Pr-Ho	1.0 mol L^{-1} KOH	η_{10} = 78 mV	24 h@−10 mA cm^{-2}	[60]
AlMnYNiCoAu	1.0 mol L^{-1} KOH	η_{10} = 124 mV	18 h@−10 mA cm^{-2}	[61]
$Mg_{80}Ni_{20}$	1.0 mol L^{-1} KOH	η_{10} = 33.1 mV	100 h@−20 mA cm^{-2}	[62]
D-NiNbIrPt	1.0 mol L^{-1} KOH	η_{10} = 19 mV	1000 h@−0.5 A cm^{-2}	[63]

变为三个原子模式, 稳定了MGNP的非晶态结构, 并防止了结晶引起的性能下降. 这种MRO结构变化不是由ORR过程中的部分表面氧化衍生而来的, 因为氧化往往会降低电催化剂的ORR性能, 而MRO结构演变有利于MGNPs在ORR中的稳定性. Pd-Ni-P MGNP在氧饱和的0.1 mol L^{-1} KOH电解液中表现出优异的电催化活性和稳定性. 在1600 r min^{-1}的起始电位和半波电位($E_{1/2}$)分别为0.96和0.84 V/RHE, 且经过1000次循环伏安测试(CV)后的极化曲线的起始电位几乎没有变化, 半波电位仅降低了10 mV, 这表明Pd-Ni-P MGNPs具有很高的稳定性(图4(d)–(f)).

3.2　氧化反应

3.2.1　析氧反应(OER)

电解水由两个半反应组成, 分别是阳极的析氧反应(OER)和阴极的析氢反应(HER)[69]. 然而, 由于OER反应涉及四电子-质子耦合反应过程, 动力学过程非常缓慢[70]. 因此, 在实际反应中, 实现电解水所施加的电极电位要远高于理论电解水动力学电位1.23 V/RHE[71]. 即使在使用催化剂的情况下, 也难以将实际电极电位降到1.23 V/RHE, 这导致制氢的能耗和成本过高[72]. 因此, OER是电解水技术发展的一个主要瓶颈, 需要开发高效的催化剂来克服OER较高的过电位. 另外, OER也受电解液pH值的影响较大[73], 其反应步骤涉及不同的反应物、产物以及各种反应中间体的吸附/脱附, 包括O*, HO*和HOO*等中间体, 也导致了OER过程的复杂性.

过渡金属Ni/Co/Fe基等非晶态合金体系同时具备廉价、3d轨道未满以及短程有序的特点, 从而使其在电解水领域成为研究热点. 2017年, Tan等人[74]探索了Ni-Fe-P非晶条带的OER性能, 原始非晶条带的OER过电位约为320 mV, 催化性能可与商业催化剂IrO_2媲美

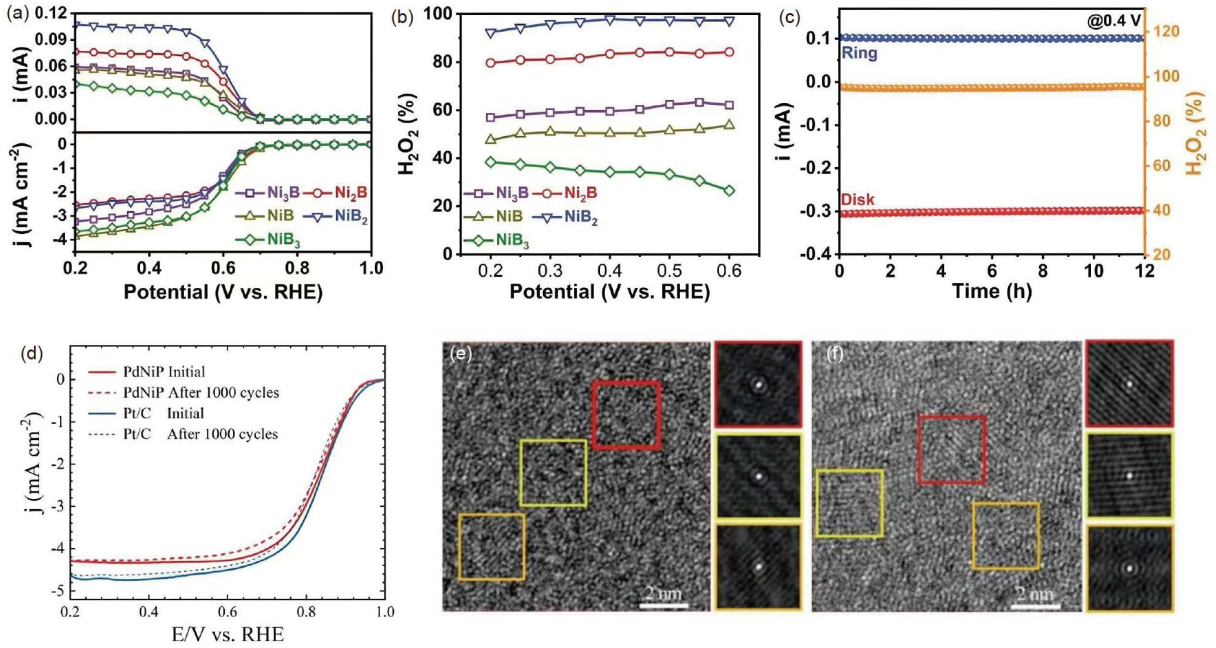

图 4　(网络版彩图) (a) Ni-B样品的LSV曲线; (b) 根据LSV曲线计算的相应H_2O_2 (%); (c) 在0.4 V/RHE条件下, NiB_2在氧饱和0.1 mol L^{-1} KOH条件下的计时电流法测试(i_{disk}为盘电流密度, i_{ring}为环电流密度)[67]; (d) Pd-Ni-P/C和Pt/C在氧饱和0.1 mol L^{-1} KOH中的LSV曲线(1600 r min^{-1}); (e), (f) Pd-Ni-P MGNPs经历1000 CV循环前(e)和1000 CV循环后(f)的HRTEM图像[68]

Figure 4　(Color online) (a) LSV curves of the Ni-B samples; (b) the calculated H_2O_2 (%) of the corresponding LSV curves; (c) chronoamperometry of NiB_2 at 0.4 V/RHE in O_2-saturated 0.1 mol L^{-1} KOH (where the disk current density (i_{disk}) together with the ring currents (i_{ring}) [67]; (d) LSV curves for Pd-Ni-P/C and Pt/C in O_2-saturated 0.1 mol L^{-1} KOH (1600 r min^{-1}); (e), (f) HRTEM images for the Pd-Ni-P MGNPs before (e) and after (f) 1000 CV cycles [68].

(η_{10} ≈ 320 mV), 通过表面处理后过电位降低至255 mV. Hu等人[75]通过对Ni-Fe-P非晶条带中的元素比例进行调控以及表面处理, 进一步提高了Ni-Fe-P非晶条带的OER性能, 过电位降低至219 mV, OER催化性能已远远优于商业催化剂. 2022年, Li等人[76]通过控制非晶形成金属液体的凝固行为, 在界面处获得了丰富的高能原子台阶. 通过调整化学成分和冷却速率, 在Fe-Ni-B金属玻璃(MG)基体中原位形成$FeNi_3$纳米晶, 从而产生有序/无序的锯齿状原子台阶界面(图5(b)–(d)). 最优的$FeNi_3$纳米晶/MG复合材料在10 mA cm^{-2}的电流密度下的过电位和Tafel斜率分别为214 mV和32.4 mV dec^{-1}, 并在碱性电解液中具有良好的稳定性(120 h) (图5(e)–(g)), 优于大多数先进的催化剂. 该方法基于对非晶形成液体中纳米晶的成核和生长速度的控制, 借助过冷状态时的动力学阻挫效应, 可以获得高度阶梯式的界面结构.

上述研究可以看出, 纳米晶/非晶复合材料可以作为一种有效的策略提升电催化性能. 纳米晶/非晶复合材料结合了丰富的催化位点和良好的导电性这两个关键因素, 是实现高性能催化剂的候选材料. 2022年, Zhang等人[77]通过$NaBH_4$水解和高温磷化(NaH_2PO_2)工艺, 成功制备了由$Fe_3P_{0.37}B_{0.63}$合金纳米颗粒修饰的非晶态Ni_2P和Fe_2P纳米片组成的FePB/NiFeP纳米晶/非晶复合催化剂. FePB/NiFeP纳米晶/非晶复合催化剂表现出优异的OER性能和稳定性, 当电流密度达到10 mA cm^{-2}时, 过电位仅为182 mV, Tafel斜率为43.9 mV dec^{-1}, 优于大多数过渡金属基OER电催化剂. 除此之外, Zhang等人[78–81]发现, 晶体材料, 尤其是高熵合金(HEA), 在电催化过程中极容易发生表面重构, 生成大量金属氧化物和局域非晶结构, 表现出优异的OER性能. 这些研究为其他先进合金催化剂的设计提供了思路. 表2[82–102]是近几年部分非晶态合金催化剂用于OER的汇总.

3.2.2　醇氧化反应(AOR)

OER是电解水整体能量转换效率的制约因素, 除

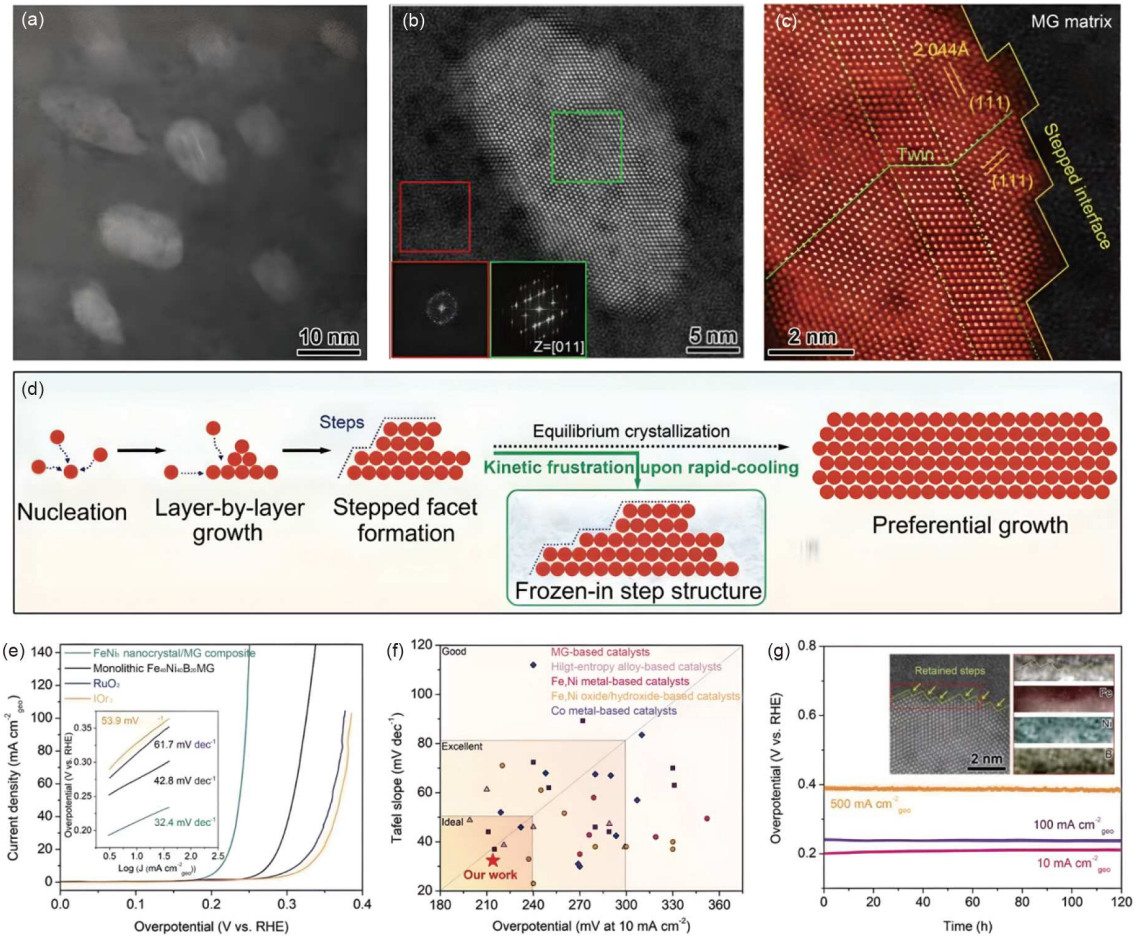

图 5　(网络版彩图) (a) 原位析出$FeNi_3$纳米晶的$Fe_{40}Ni_{40}B_{20}$ MG复合材料HRTEM图像; (b) $FeNi_3$纳米晶的HAADF-STEM图像, 插图显示了所选区域的FFT模式; (c) $FeNi_3$纳米晶与MG基体间阶梯界面的原子结构; (d) 阶梯界面结构在快速凝固过程中的形成过程示意图; (e) OER极化曲线; (f) $FeNi_3$纳米晶/MG复合材料与最近报道的各种过渡金属基电催化剂在碱性电解液中的OER活性比较; (g) 计时电位曲线[76]

Figure 5　(Color online) (a) HRTEM image of the as-spun $Fe_{40}Ni_{40}B_{20}$ MG composite with *in situ* precipitated $FeNi_3$ nanocrystals; (b) HAADF-STEM image of the $FeNi_3$ nanocrystal, the insets show the FFT patterns of the selected areas; (c) atomic structure of the stepped interface between the twined $FeNi_3$ nanocrystal and MG matrix; (d) schematic illustration of the formation process of the stepped interface architecture during rapid solidification; (e) OER polarization curves; (f) comparison of the OER activity of the $FeNi_3$ nanocrystal/MG composite with various recently reported transition metal-based electrocatalysts in alkaline; (g) chrono-potentiometric curves [76].

了开发低成本、高效率的OER催化剂外, 利用热力学反应势垒更低的醇氧化反应(AOR)来替代OER被认为是解决阳极氧化瓶颈的一种策略[103]. 这种替代可以在阳极产生比O_2更有价值的化学物质. 甲醇氧化反应(MOR)和乙醇氧化反应(EOR)是替代OER的有效阳极反应, 因为它们需要的电位很低[104]. 此外, MOR避免了H_2与O_2的混合并防止制备过程中发生爆炸的风险, 也无需进行气体分离即可生产纯氢气. 除此之外, 直接醇燃料电池(DAFC)也可作为解决全球环境问题和能源问题的一条可行途径. 然而, 由于阳极反应(AOR)动力学缓慢, 也阻碍了DAFC的广泛应用[105]. 目前的晶态催化剂通常存在催化效率低、CO中毒严重和活性衰减快等问题, 极大地限制了其实际应用[106]. 因此, 开发高活性和稳定性的非晶态合金催化剂用于提高AOR氧化反应效率是一个极具前景的策略.

2018年, Xu等人[19]通过电化学脱合金工艺实现选择性地溶解具有低“分离极限”的$Au_{55}Cu_{25}Si_{20}$金属玻璃条带中的一种元素, 形成三维“圆锥形突起”纳米多孔结构. 一方面, 这种3D多孔结构提供了高密度的本征催化位点, 因为“锥形突起”内部在凹凸区域之间具

表 2　非晶态合金的OER催化性能

Table 2　OER catalytic performance of amorphous alloys

催化剂	电解液	过电位	稳定性测试	文献
FeCoNiMoVO	1.0 mol L^{-1} KOH 海水	η_{10} = 216 mV η_{10} = 236 mV	100 h@1 A cm^{-2}	[82]
FeCoMoPB	1.0 mol L^{-1} KOH	η_{10} = 239 mV	48 h@10 mA cm^{-2}	[83]
$Ni_{28}Fe_{42}Mn_{30}$	1.0 mol L^{-1} KOH	η_{100} = 282 mV	100 h@100 mA cm^{-2}	[84]
$Ni_{40}Fe_{40}B_{20}$	1.0 mol L^{-1} KOH	η_{10} = 319 mV	24 h@10 mA cm^{-2}	[85]
$Fe_{50}Ni_{27}Nb_3P_{13}C_7$	6.0 mol L^{-1} KOH	η_{10} = 248 mV	18 h@10 mA cm^{-2}	[86]
$FeCoNiCrMo_x$	1.0 mol L^{-1} KOH	η_{100} = 294.5 mV	160 h@100 mA cm^{-2}	[87]
FeCoNiMoPB	1.0 mol L^{-1} KOH	η_{10} = 281 mV	107 h@10 mA cm^{-2}	[88]
$Fe_{40}Co_{40}B_{20}$	1.0 mol L^{-1} KOH	η_{10} = 315 mV	24 h@10 mA cm^{-2}	[89]
$Ni_{50}Fe_{25}B_{15}Si_7P_3$	1.0 mol L^{-1} KOH	η_{10} = 235 mV	80 h@10 mA cm^{-2}	[90]
Co-W-B	1.0 mol L^{-1} KOH	η_{10} = 292 mV	10 h@300 mV	[91]
FeNiCo-ANs	1.0 mol L^{-1} KOH	η_{10} = 274 mV	10 h@30 mA cm^{-2}	[92]
$Fe_{78}Si_9B_{13}$	1.0 mol L^{-1} KOH	η_{10} = 240 mV	48 h@10 mA cm^{-2}	[93]
$Ni_{40}Fe_{40}B_{20}$	1.0 mol L^{-1} KOH	η_{10} = 249 mV	100 h@100 mA cm^{-2}	[94]
$Fe_{40}Ni_{20}Co_{20}P_{15}C_5$	1.0 mol L^{-1} KOH	η_{10} = 236 mV	20 h@330 mV	[95]
NiFeCoP	1.0 mol L^{-1} KOH	η_{10} = 245 mV	20 h@10 mA cm^{-2}	[96]
$(FeCoNi)_{80}P_{14}B_6$	1.0 mol L^{-1} HCl	η_{10} = 229 mV	25 h@350 mA cm^{-2}	[97]
FeNiCoP	1.0 mol L^{-1} NaOH	η_{10} = 281 mV	20 h@10 mA cm^{-2}	[98]
$(Fe_{73.5}Si_{13.5}B_9Nb_3Cu_1)_{91.5}Ni_{8.5}$	1.0 mol L^{-1} KOH	η_{10} = 230 mV	–	[99]
$(Ni_{0.4}Fe_{0.4}B_{0.2})_{100-x}Ru_x$	1.0 mol L^{-1} KOH	η_{10} = 245 mV	15 h@10 mA cm^{-2}	[100]
$Ir_{25}Ni_{33}Ta_{42}$	1.0 mol L^{-1} KOH	η_{10} = 266 mV	10 h@10 mA cm^{-2}	[101]
$Fe_{29}Co_{27}Ni_{23}Si_9B_{12}$ HEA	1.0 mol L^{-1} KOH	η_{10} = 230 mV	50 h@100 mA cm^{-2}	[102]

有较大的曲率梯度，并且具有大量的低配位原子位点. 另一方面，理论和实验工作已经表明，弹性应变可以增强分子相互作用, 从而减少化学反应的能垒. 因此, 多孔“锥形突起”内部结构和应变效应的相互作用可有效提高电催化能力. 当甲醇浓度增加到2 mol L^{-1}时，甲醇氧化电位峰负向偏移至0.31 V/Ag/AgCl, 最优的MOR活性达到232.5 μA cm^{-2}. 除了MOR行为, $Au_{55}Cu_{25}Si_{20}$金属玻璃电极还具有更优异的EOR电化学性能. 当乙醇浓度增加到2 mol L^{-1}时，EOR的起始电位从−0.05 V/Ag/AgCl负向偏移到−0.18 V/Ag/AgCl，最大活性从451 μA cm^{-2}提高到928 μA cm^{-2}. 另外，2020年，Baksi等人[107]也报道了$Ni_{60}Nb_{40}$金属玻璃具有较高的MOR性能.

3.2.3　尿素氧化反应(UOR)

由于四电子反应的动力学缓慢，阳极的OER在很大程度上阻碍了制氢效率. 除了开发上述AOR催化剂可以代替OER外，也可以用热力学势垒较低的其他电化学氧化反应(如尿素/氨/生物质氧化)代替OER，这也被认为是实现节能制氢的可行方法[108]. 通常，尿素广泛存在于不同的废水(如人类尿液、工业废水)中[109]，因此尿素氧化反应(UOR)工艺不仅是高效制氢的关键反应[110]，还可以净化各种含尿素废水，这对经济和环境都具有重要意义. 为了降低UOR能耗，开发用于UOR的高效催化剂是当务之急.

Pei等人[20]证明了电沉积的Ni-P纳米玻璃(NG)由于其异质结构而具有极高的能态，而催化性能将受益于高能量状态. 特别是较高的表面能等效于较高的活性，该活性来自催化剂表面较多的低配位位点. 而且，具有异质结构的Ni-P NG是制备独特的蜂窝状纳米孔结构的完美前驱体, 在UOR中表现出优异的催化性能. 具体来说，优化后的Ni-P NG在电流密度达到10 mA cm^{-2}时仅需要1.36 V/RHE的电位，Tafel斜率仅为13 mV dec^{-1}，UOR性能远优于其他镍基合金. 除此之外，Ni-P NG在1.0 mol L^{-1} KOH溶液中也具有很好的OER性能，即在电流密度达到10 mA cm^{-2}时仅需要1.54 V/RHE的电位(图6(a)–(e)). 2024年, Sohel等人[111]报道了$Ni_{60}Nb_{40}$纳米玻璃异质界面作为一种有前途的无黏结剂、自支撑电极UOR催化剂. 通过原位生成稳

定的γ-NiOOH活性物质促进了氧化, 在1.0 mol L^{-1} KOH的碱性电解液中, $Ni_{60}Nb_{40}$纳米玻璃在施加电位下表面易原位生成γ-NiOOH, 这进一步有效控制了UOR动力学, Tafel斜率低至16 mV dec^{-1}, 并且在38 mA cm^{-2}的电流密度下可进行长达70 h的长电催化反应, 表明了其优异的稳定性, 这归因于纳米结构的玻璃界面促进了更多γ-NiOOH物种的形成. 表面稳定的$Ni_{60}Nb_{40}$纳米玻璃也表现出类似的机制, 独特的纳米结构、玻璃颗粒和界面的存在导致了高活性物种的产生.

3.3　非晶态合金催化剂在污水处理领域的应用

纺织工业废水逐渐成为一个严峻的环境问题, 从废水中去除染料在环境工程方面具有巨大的发展潜力[112]. 目前, 全球每年生产超过70万吨有机染料, 其中偶氮染料的种类高达10000多种, 约占商业染料总产量的60%–70%[113], 这类偶氮染料通常具有各种颜色. 偶氮染料具有高度耐久性、毒性, 并可在生物体内累积, 对生物体和人类产生较大的威胁[114]. 据报道, 只有45%–47%的有机染料可以生物降解并溶解于水, 其余53%–55%的偶氮染料是有害的[26], 它们的降解已成为一个紧迫的问题. 为了开发有效的技术来降解和净化被染料污染的水体, 人们尝试了各种催化剂来修复染料废水[115]. 虽然各种纳米催化剂相继被开发, 但是这些纳米催化剂的循环使用次数极其有限, 其分离难度大[116]也限制了它们的实际应用.

2020年, Miao等人[117]报道了FeBC非晶条带对酸性橙7 (AO7)具有高效降解能力, 并将其与FePC非晶条带进行了比较(图7(a)–(d)). 使用FeBC非晶条带降解50%的AO7所需的时间仅为使用FePC条带的1/3. 在FeBC非晶基体中, 由于Fe–B键和Fe–C键之间的键合强度差异大, 形成了原电池结构, 这导致FeBC非晶条带的反应活化能低且降解效率高. FeBC非晶条带不仅在酸性条件下具有优异的AO7降解能力, 而且在中性和弱碱性环境中也均具有优异的降解能力. 2022年, Peng等人[118]利用沉积过程中的可控表面扩散和抑制晶体粗化过程, 利用具有纳米级相分离的MG薄膜前体制备了致密非晶-晶体(a/c)复合界面的超细a/c FeSiBNb催化剂. 该超细a/c催化剂表现出优异的循环降解

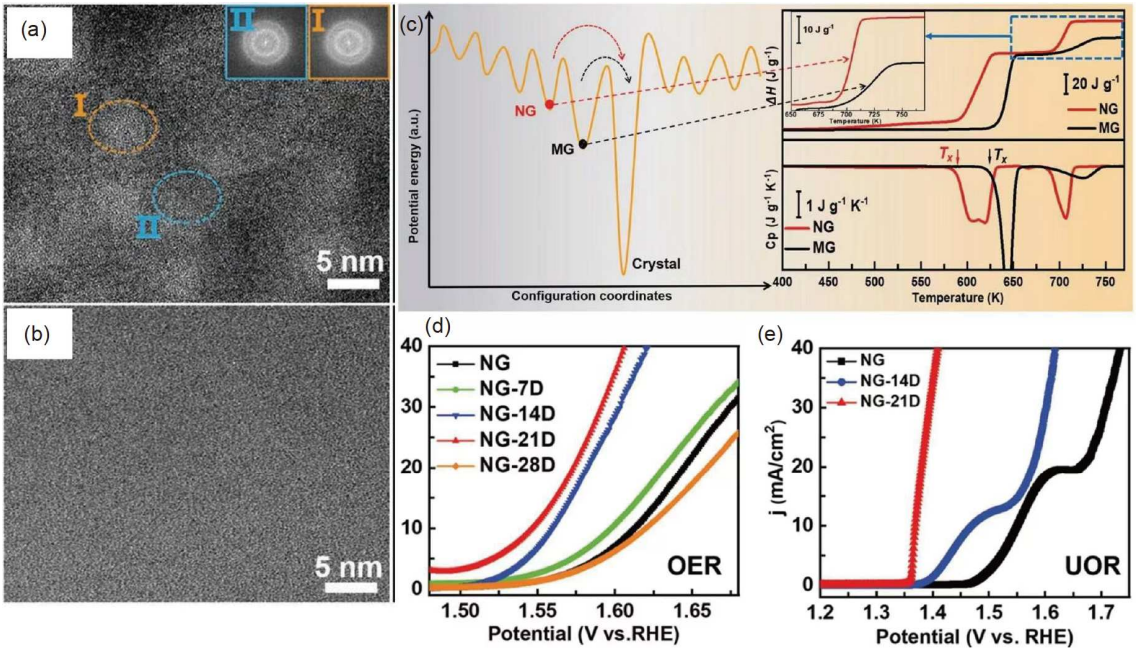

图 6　(网络版彩图) (a), (b) NG (a)和MG (b)的HRTEM图像. (c) 左图是NG和MG的势能分布示意图. 右下方图为加热速率为20 K min^{-1}时NG和MG的热容曲线. 右上方图是由NG和MG热容曲线积分得到的焓变(ΔH)曲线, 其中插图是ΔH曲线的放大图像. (d) OER极化曲线. (e) UOR极化曲线[20]

Figure 6　(Color online) (a), (b) HRTEM images of NG (a) and MG (b). (c) The left is a schematic diagram of the potential energy landscape of the NG and MG. Heat capacity curves of the MG and NG are exhibited on the lower right for the heating rate of 20 K min^{-1}. Enthalpy change (ΔH) curves obtained by the integration of the heat capacity curves are displayed on the top right, where the insert is the enlarged image of the ΔH curves. (d) OER polarization curves. (e) UOR polarization curves [20].

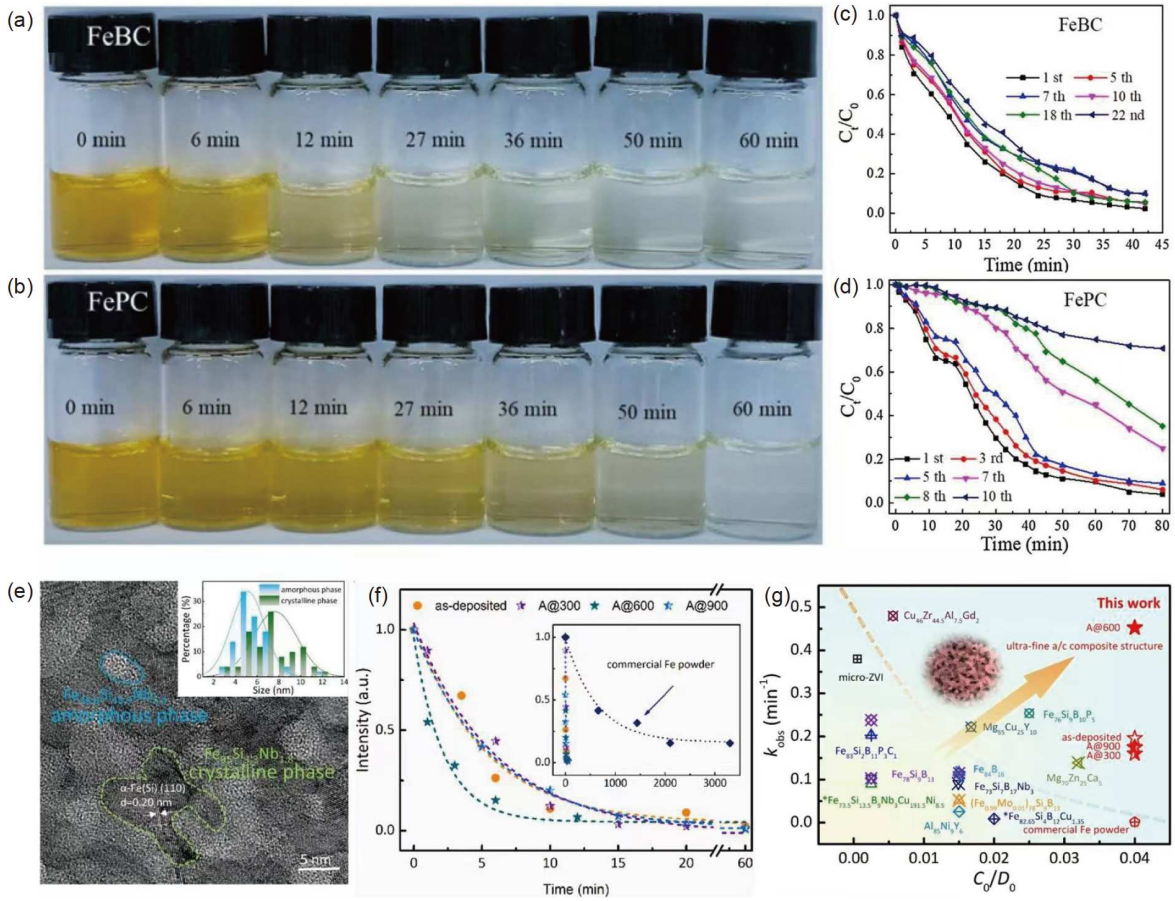

图 7　(网络版彩图) (a), (b) 使用FeBC (a)和FePC (b)降解AO7溶液的颜色变化. (c), (d) FeBC (c)和FePC (d)条带在不同降解时间下AO7溶液的归一化浓度变化[117]. (e) A@600薄膜的HRTEM图像, 插图显示了非晶相和晶相的尺寸分布. (f) 588 nm波长附近的归一化吸收强度与处理时间的关系, 插图显示了与商用铁粉的降解行为比较. (g) 染料降解性能比较(不包括Fenton类反应). 不同金属玻璃和晶态零价铁催化剂的降解率与用量比[118]

Figure 7　(Color online) (a), (b) Visible color change of AO7 solution degraded by FeBC (a) and FePC (b) amorphous ribbons. (c), (d) The normalized concentration change of AO7 solutions at different degradation cycles of FeBC (c) and FePC (d) ribbons [117]. (e) HRTEM image of A@600 film, the inset shows the size distribution of the amorphous phase and crystalline phase. (f) Normalized absorption intensities around 588 nm as a function of the treatment time, the inset shows the comparison degradation behavior with commercial Fe powder. (g) Comparison of dye degradation performance (Fenton-like reactions are not included). Degradation rate *versus* dosage ratio for different metallic glasses and crystalline ZVI catalysts [118].

性能和染料降解效率, 是商业铁粉的300倍(图7(e)–(g)). 特别是a/c复合材料无需额外加入H_2O_2即可实现出色的催化性能, 这不仅提供了环保的中性催化条件, 还避免了商业污水处理过程中的腐蚀损害.

4　非晶态合金在催化领域面临的问题与展望

催化反应的研究重点是探索高效耐用的催化剂. 虽然大部分研究都集中在晶体材料上, 但非晶态合金催化剂在降低成本和提高电化学效率方面展现出显著优势. 与晶态催化剂相比, 非晶态合金催化剂具有更多的活性位点, 大量的固有缺陷也有利于提高其催化活性. 这些优点使得非晶态合金在电化学领域具有很强的吸引力. 虽然非晶态合金在催化领域的应用前景广阔, 但相关研究仍处于起步阶段. 可以预见, 随着人们对各种合成方法的掌握, 以及各种高端表征技术的兴起和利用, 非晶态合金催化剂的研究将会取得更多重大进展. 在此, 我们总结了非晶态合金催化剂面临的一些科学问题, 并对未来的研究进行了展望.

(1) 合成方法: 传统的非晶态合金制备方法通常需要高温、高压和复杂的工艺, 这导致了制备过程可控性差和成本较高. 因此, 开发简单、高效且可大规模应用的制备方法是非常重要的. 随着3D打印技术的兴起, 其在材料制备方面具有成本低、精度高和结构可控等优势, 这使得非晶态合金在催化领域的合成技术有望实现突破.

(2) 材料筛选: 目前, 非晶态合金催化剂的研发和设计主要依赖于经验和反复试验. 为了降低成本和缩短实验周期, 机器学习(ML)方法的最新进展已证明其在预测非晶态合金性能方面的有效性和实用性, 特别是在催化剂设计领域. 与第一性原理计算相比, 机器学习方法使物质的采样和分析变得更加广泛和系统. 机器学习是加速催化剂研究的有力工具, 它能够高精度地建立模型, 预测未知催化剂的催化性能, 并揭示催化剂的结构与性能之间的关系. 机器学习模型成功的关键在于使用合适且通用的描述符, 以准确、全面和系统地表示非晶态合金催化剂的结构信息.

(3) 相比于晶态催化剂, 人们对非晶态合金催化剂的认识仍然不够. 虽然大量文献报道了非晶态合金催化剂的催化性能优于同组分的晶态催化剂, 但其确切原因仍然不清楚. 因此, 亟须开发更多先进的表征技术和理论手段, 以探索其结构与催化性能之间的构效关系, 丰富和发展非晶态合金催化剂的物理化学理论.

(4) 原位表征手段: 与晶态催化剂相比, 非晶态合金中缺乏明确的远程有序结构, 这导致催化机理更加复杂. 因此, 需要发展先进的表征技术和理论方法, 以揭示非晶态合金催化剂的催化反应机理. 原位表征技术, 如原位傅里叶变换红外光谱(*in-situ* FTIR)、原位拉曼光谱(*in-situ* Raman)、原位X射线衍射分析(*in-situ* XRD)、原位透射电子显微镜(*in-situ* TEM)、原位球差校正透射电子显微镜(*in-situ* ACTEM)、原位电子能量损失谱(*in-situ* EELS)、原位X射线光电子能谱(*in-situ* XPS)、原位微分电化学质谱(*in-situ* DEMS)和原位同步辐射(*in-situ* XAS)等, 对于检测催化剂表面关键中间体的吸附和脱附, 以及化学键的形成和断裂至关重要. 这些技术有助于我们更好地了解活性位点的形成和演变, 并在原子尺度上建立精确的结构-性能关系, 解析催化反应的物化机制, 为非晶态合金催化剂的结构优化提供指导.

(5) 定向表面重构: 非晶态物质具有亚稳态结构, 在极端物理或化学条件下易发生表面重构, 转变为晶体结构, 这会影响催化活性和稳定性. 由于非晶态合金在电化学环境中往往会重构生成晶体层, 形成纳米/非晶复合材料, 这极有可能提升电化学性能, 但该过程的不可控性也增加了研究的难度. 因此, 迫切需要从实验结果和理论出发, 发展新的策略, 使非晶态合金催化剂能够定向重构, 从而提升其催化性能和稳定性.

(6) 构筑纳米-非晶异质结: 纳米-非晶异质结催化剂具有独特的结构优势. 非晶结构通常具有更高的表面能和更多的活性位点, 而纳米晶则具有更好的热稳定性和导电性. 通过晶化工程或非晶化工程构筑纳米-非晶异质结构, 或者将非晶态合金与纳米晶材料直接复合以构筑异质结, 结合两者的优点, 可以实现更高效的催化性能.

目前, 对非晶态合金特性的研究大多集中在力学和磁性领域. 近几年的研究表明, 非晶态合金在催化领域表现出优异的性能. 随着非晶态合金在合成、表征和理论计算等方面的快速发展, 预计将在能源储存和转换领域发挥重大作用.

参考文献

1 Kramer J. Über nichtleitende metallmodifikationen. Ann Phys, 1934, 411: 37–64

2 Brenner A, Couch D E, Williams E K. Electrodeposition of alloys of phosphorus with nickel or cobalt. J Res Natl Bur Stan, 1950, 44: 109

3 Cohen M H, Turnbull D. Molecular transport in liquids and glasses. J Chem Phys, 1959, 31: 1164–1169

4 Klement Jun. W, Willens R H, Duwez P. Non-crystalline structure in solidified gold-silicon alloys. Nature, 1960, 187: 869–870

5 Dyre J C. Colloquium: The glass transition and elastic models of glass-forming liquids. Rev Mod Phys, 2006, 78: 953–972

6 Wang W H. The nature and properties of amorphous matter (in Chinese). Rep Prog Phys, 2013, 33: 177–351 [汪卫华. 非晶态物质的本质和特性. 物理学进展, 2013, 33: 177–351]

7 Wang W H. Development and implication of amorphous alloys (in Chinese). Bull Chin Acad Sci, 2022, 37: 352–359 [汪卫华. 非晶态合金材料发展趋势及启示. 中国科学院院刊, 2022, 37: 352–359]

8 Meng S, Wang Z, Zhu R, et al. Near-perfect replication on amorphous alloys through active force modulation based on machine learning/neural network parameter prediction. Sci China-Phys Mech Astron, 2025, 68: 216111

9 Smith G V, Brower W E, Matyjaszczyk M S. Metallic glasses: New catalyst systems. Stud Surf Sci Catal, 1981, 7: 355–363

10 Brower Jr W E, Matyjaszczyk M S, Pettit T L, et al. Metallic glasses as novel catalysts. Nature, 1983, 301: 497–499

11 van Wonterghem J, Mørup S, Koch C J W, et al. Formation of ultra-fine amorphous alloy particles by reduction in aqueous solution. Nature, 1986, 322: 622–623

12 Zong B N, Min E Z, Dong S Z, et al. Studies of amorphous metals as catalytic material I. Catalytic hydrogenation of styrene on amorphous Ni-P (in Chinese). Acta Chim Sin, 1989, 11: 1052–1055 [宗保宁, 闵恩泽, 董树忠, 等. 非晶态金属合金作催化材料的研究I. Ni-P非晶态合金对苯乙烯加氢活性的研究. 化学学报, 1989, 11: 1052–1055]

13 Lian K, Thorpe S J, Kirk D W. Electrochemical and surface characterization of electrocatalytically active amorphous Ni-Co alloys. Electrochim Acta, 1992, 37: 2029–2041

14 Yang J, Cui L L, Deng J F. Catalytic properties of nanosize Ni-B amorphous alloy (in Chinese). Chem J Chin Univ, 1994, 12: 1848–1850 [杨军, 崔黎丽, 邓景发. 纳米Ni-B非晶态合金的催化性质研究. 高等学校化学学报, 1994, 12: 1848–1850]

15 Kleinke M U, Knobel M, Bonugli L O. Amorphous alloys as anodic and cathodic materials for alkaline water electrolysis. Int J Hydrogen Energy, 1997, 22: 759–762

16 Ramos-Sánchez G, Pierna A R, Solorza-Feria O. Amorphous $Ni_{59}Nb_{40}Pt_xM_{1-x}$ (M = Ru, Sn) electrocatalysts for oxygen reduction reaction. J Non-Cryst Solids, 2008, 354: 5165–5168

17 Zhang C, Zhang H, Lv M, et al. Decolorization of azo dye solution by Fe-Mo-Si-B amorphous alloy. J Non-Cryst Solids, 2010, 356: 1703–1706

18 Jiang R, Tran D T, McClure J P, et al. A class of (Pd-Ni-P) electrocatalysts for the ethanol oxidation reaction in alkaline media. ACS Catal, 2014, 4: 2577–2586

19 Xu Y, Cheng J, Yiu P M, et al. Evolution of 3D nanoporosity and morphology in selectively dealloying ternary $Au_{55}Cu_{25}Si_{20}$ metallic glass ribbon with enhanced alcohol electro-oxidation performance. Nanoscale, 2018, 10: 18846–18856

20 Pei C, Chen S, Zhao T, et al. Nanostructured metallic glass in a highly upgraded energy state contributing to efficient catalytic performance. Adv Mater, 2022, 34: 2200850

21 Gao F Y, Liu S N, Ge J C, et al. Nickel-molybdenum-niobium metallic glass for efficient hydrogen oxidation in hydroxide exchange membrane fuel cells. Nat Catal, 2022, 5: 993–1005

22 Ding Y, Song L, Wang Z, et al. Unveiling the time-temperature dependence of metastability of supercooled liquid using nano-calorimetry. Sci China-Phys Mech Astron, 2024, 67: 236113

23 Zhang B, Zhao Y, Bai H Y. Stability of metallic glasses. Physics, 2022, 51: 709–716

24 Cai W, Chen R, Yang H, et al. Amorphous *versus* crystalline in water oxidation catalysis: A case study of NiFe alloy. Nano Lett, 2020, 20: 4278–4285

25 Anantharaj S, Noda S. Amorphous catalysts and electrochemical water splitting: An untold story of harmony. Small, 2020, 16: 1905779

26 Zhang L C, Jia Z, Lyu F, et al. A review of catalytic performance of metallic glasses in wastewater treatment: Recent progress and prospects. Prog Mater Sci, 2019, 105: 100576

27 Li X, Cai W, Li D S, et al. Amorphous alloys for electrocatalysis: The significant role of the amorphous alloy structure. Nano Res, 2023, 16: 4277–4288

28 Chen Y, Sun H, Guo J, et al. Research on carbon-based and metal-based negative electrode materials via DFT calculation for high potassium storage performance: A review. Energy Mater, 2023, 3: 300044

29 Yang Y, Li P, Zheng X, et al. Anion-exchange membrane water electrolyzers and fuel cells. Chem Soc Rev, 2022, 51: 9620–9693

30 Rosen M A, Koohi-Fayegh S. The prospects for hydrogen as an energy carrier: An overview of hydrogen energy and hydrogen energy systems. Energ Ecol Environ, 2016, 1: 10–29

31 Davis E M, Bergmann A, Kuhlenbeck H, et al. Facet dependence of the oxygen evolution reaction on Co_3O_4, $CoFe_2O_4$, and Fe_3O_4 epitaxial film electrocatalysts. J Am Chem Soc, 2024, 146: 13770–13782

32 Ram R, Xia L, Benzidi H, et al. Water-hydroxide trapping in cobalt tungstate for proton exchange membrane water electrolysis. Science, 2024, 384: 1373–1380

33 Al-Naggar A H, Shinde N M, Kim J S, et al. Water splitting performance of metal and non-metal-doped transition metal oxide electrocatalysts.

Coord Chem Rev, 2023, 474: 214864
34 Feidenhans'l A A, Regmi Y N, Wei C, et al. Precious metal free hydrogen evolution catalyst design and application. Chem Rev, 2024, 124: 5617–5667
35 Zhang F, Wu J, Jiang W, et al. New and efficient electrocatalyst for hydrogen production from water splitting: Inexpensive, robust metallic glassy ribbons based on iron and cobalt. ACS Appl Mater Interfaces, 2017, 9: 31340–31344
36 Chu F, Han B, Edalati K, et al. Severe plastic deformed Pd-based metallic glass for superior hydrogen evolution in both acidic and alkaline media. Scr Mater, 2021, 204: 114145
37 Wang Z, Li M, Yu J, et al. Low-iridium-content IrNiTa metallic glass films as intrinsically active catalysts for hydrogen evolution reaction. Adv Mater, 2020, 32: 1906384
38 Voiry D, Chhowalla M, Gogotsi Y, et al. Best practices for reporting electrocatalytic performance of nanomaterials. ACS Nano, 2018, 12: 9635–9638
39 Jia Z, Nomoto K, Wang Q, et al. A self-supported high-entropy metallic glass with a nanosponge architecture for efficient hydrogen evolution under alkaline and acidic conditions. Adv Funct Mater, 2021, 31: 2101586
40 Tian J, Hu Y, Lu W, et al. Dealloying of an amorphous TiCuRu alloy results in a nanostructured electrocatalyst for hydrogen evolution reaction. Carbon Energy, 2023, 5: e322
41 Zou Y, Jing L, Zhang J, et al. ALD-made noble metal high entropy alloy nanofilm with sub-surface amorphization for enhanced hydrogen evolution. J Mater Chem A, 2024, 12: 5668–5678
42 Pan M, Feng H, Zhang Z, et al. Observation of a robust catalyst support based on metallic glass for large current-density water electrolysis. J Mater Chem A, 2024, 12: 15334–15342
43 Qin J, Zhang H, Lu W, et al. Nanoporous NiPt alloy by dealloying of amorphous NiZrPt metallic glass for alkaline hydrogen evolution reaction. Chem Eng J, 2024, 490: 151700
44 Jian X, Zhang W, Yang Y, et al. Amorphous Cu-W alloys as stable and efficient electrocatalysts for hydrogen evolution. ACS Catal, 2024, 14: 2816–2827
45 Zhang T, Ren X, Mo S, et al. Modulating Fe/P ratios in Fe-P alloy through smelting reduction for long-term electrocatalytic overall water splitting. J Mater Sci Tech, 2024, 199: 66–74
46 Silviya R, Bhide A, Gupta S, et al. Bifunctional amorphous transition-metal phospho-boride electrocatalysts for selective alkaline seawater splitting at a current density of 2 A cm^{-2}. Small Methods, 2024, 8: 2301395
47 Sun W H, Hua Y Q, Zhang X. Assembly of amorphous CoP electrocatalysts on flexible polyester textile for alkaline hydrogen evolution reaction. Int J Hydrogen Energy, 2024, 63: 28–35
48 Shi Y, Zhou S, Liu J, et al. An integrated amorphous cobalt phosphoselenide electrocatalyst with high mass activity boosts alkaline overall water splitting. Appl Catal B-Environ, 2024, 341: 123326
49 Yan M, Chen S, Wu S, et al. Enhanced activity and durability of FeCoCrMoCBY nanoglass in acidic hydrogen evolution reaction. J Mater Sci Tech, 2024, 170: 212–220
50 Li Y, Tang J, Zhang H, et al. *In-situ* construction and repair of high catalytic activity interface on corrosion-resistant high-entropy amorphous alloy electrode for hydrogen production in high-temperature dilute sulfuric acid electrolysis. Chem Eng J, 2023, 453: 139905
51 Jia Z, Yang Y, Wang Q, et al. An ultrafast and stable high-entropy metallic glass electrode for alkaline hydrogen evolution reaction. ACS Mater Lett, 2022, 4: 1389–1396
52 Zhang X, Yang Y, Liu Y, et al. Defect engineering of a high-entropy metallic glass surface for high-performance overall water splitting at ampere-level current densities. Adv Mater, 2023, 35: 2303439
53 Chu F, Wu K, Meng Y, et al. Effect of high-pressure torsion on the hydrogen evolution performances of a melt-spun amorphous $Fe_{73.5}Si_{13.5}B_9Cu_1Nb_3$ alloy. Int J Hydrogen Energy, 2021, 46: 25029–25038
54 Jiang S, Zhu L, Yang Z, et al. Self-supported hierarchical porous FeNiCo-based amorphous alloys as high-efficiency bifunctional electrocatalysts toward overall water splitting. Int J Hydrogen Energy, 2021, 46: 36731–36741
55 Jiang S, Zhu L, Yang Z, et al. Morphological-modulated FeNi-based amorphous alloys as efficient alkaline water splitting electrocatalysts. Electrochim Acta, 2021, 389: 138756
56 Shao G, Wang Q, Miao F, et al. Improved catalytic efficiency and stability by surface activation in Fe-based amorphous alloys for hydrogen

evolution reaction in acidic electrolyte. Electrochim Acta, 2021, 390: 138815
57 Aneeshkumar K S, Tian J, Shen J. Dual-phase amorphous-nanocrystalline nanoporous sites activated in Mo inserted CuTi metallic glass as efficient electrocatalysts for hydrogen evolution reaction. J Alloys Compd, 2021, 886: 161270
58 Jo W, Jeong D, Jeong J, et al. Electrocatalytic properties of pulse-reverse electrodeposited nickel phosphide for hydrogen evolution reaction. Front Chem, 2021, 9: 781838
59 Yuan F H, Mohammadi M R, Ma L L, et al. Electrodeposition of self-supported NiMo amorphous coating as an efficient and stable catalyst for hydrogen evolution reaction. Rare Met, 2022, 41: 2624–2632
60 Liu W, Tan W, He H, et al. One-step electrodeposition of Ni-Ce-Pr-Ho/NF as an efficient electrocatalyst for hydrogen evolution reaction in alkaline medium. Energy, 2022, 250: 123831
61 Zou P, Zang B, Song L, et al. Nanoporous AlMnYNiCoAu catalysts for hydrogen evolution. ACS Appl Nano Mater, 2022, 5: 17673–17681
62 Xu H, Wang X, Zhao W, et al. Facile self-oxidized Ni nano-foam as high-performance catalyst for hydrogen and oxygen evolution. Sci China Mater, 2023, 66: 3855–3864
63 Zhang Y, Li R, Wang X, et al. Surface active-site engineering of low-noble-metal-alloyed metallic glass catalyst for boosting water electrolysis. Adv Funct Mater, 2024, 34: 2410379
64 Zhang W, Li J, Wei Z. Carbon-based catalysts of the oxygen reduction reaction: Mechanistic understanding and porous structures. Chin J Catal, 2023, 48: 15–31
65 Hu J, Liu W, Xin C, et al. Carbon-based single atom catalysts for tailoring the ORR pathway: A concise review. J Mater Chem A, 2021, 9: 24803–24829
66 Zhao W, Xu G, Dong W, et al. Progress and perspective for *in situ* studies of oxygen reduction reaction in proton exchange membrane fuel cells. Adv Sci, 2023, 10: 2300550
67 Wu J, Hou M, Chen Z, et al. Composition engineering of amorphous nickel boride nanoarchitectures enabling highly efficient electrosynthesis of hydrogen peroxide. Adv Mater, 2022, 34: 2202995
68 Fu S, Chen G, Guo H, et al. Synthesis of free-standing Pd-Ni-P metallic glass nanoparticles with durable medium-range ordered structure for enhanced electrocatalytic properties. Small, 2023, 19: 2300721
69 Chang J, Shi Y, Wu H, et al. Oxygen radical coupling on short-range ordered Ru atom arrays enables exceptional activity and stability for acidic water oxidation. J Am Chem Soc, 2024, 146: 12958–12968
70 Jiang Q, Wang S, Zhang C, et al. Active oxygen species mediate the iron-promoting electrocatalysis of oxygen evolution reaction on metal oxyhydroxides. Nat Commun, 2023, 14: 6826
71 Tian C, Liu R, Zhang Y, et al. Ru-doped functional porous materials for electrocatalytic water splitting. Nano Res, 2024, 17: 982–1002
72 Ren J T, Chen L, Wang H Y, et al. Water electrolysis for hydrogen production: From hybrid systems to self-powered/catalyzed devices. Energy Environ Sci, 2024, 17: 49–113
73 Tahir M, Pan L, Idrees F, et al. Electrocatalytic oxygen evolution reaction for energy conversion and storage: A comprehensive review. Nano Energy, 2017, 37: 136–157
74 Tan Y, Zhu F, Wang H, et al. Noble-metal-free metallic glass as a highly active and stable bifunctional electrocatalyst for water splitting. Adv Mater Inter, 2017, 4: 1601086
75 Hu F, Zhu S, Chen S, et al. Amorphous metallic NiFeP: A conductive bulk material achieving high activity for oxygen evolution reaction in both alkaline and acidic media. Adv Mater, 2017, 29: 1606570
76 Li R, Wu R, Li Z, et al. Boosting oxygen-evolving activity via atom-stepped interfaces architected with kinetic frustration. Adv Mater, 2023, 35: 2206890
77 Zhang X, Li Y, Wu Z, et al. Crystalline/amorphous composite interface induced by $NaBH_4$ hydrolysis reaction: A new interfacial electrocatalyst for efficient oxygen evolution reaction. Mater Today Energy, 2022, 26: 100987
78 Zhang T, Zhao H F, Wang K Y, et al. Three factors make bulk high-entropy alloys as effective electrocatalysts for oxygen evolution. Mater Futures, 2023, 2: 045101
79 Zhao H, Yao J, Wang Y, et al. Crystal facets-activity correlation for oxygen evolution reaction in compositional complex alloys. Adv Sci, 2024, 11: 2404095
80 Chen Z, Zhang T, Gao X, et al. Engineering microdomains of oxides in high-entropy alloy electrodes toward efficient oxygen evolution. Adv

Mater, 2021, 33: 2101845
81 Zhang T, Gao N, Chen Z J, et al. Grain-boundary-activity correlation for electrocatalytic oxygen evolution in high-entropy alloys. PRX Energy, 2023, 2: 033011
82 Feng C, Zhou Y, Xie Z, et al. Vanadium boosted high-entropy amorphous FeCoNiMoV oxide for ampere-level seawater oxidation. Chem Eng J, 2024, 495: 153408
83 Wang Q, Jia Z, Li J, et al. Attractive electron delocalization behavior of FeCoMoPB amorphous nanoplates for highly efficient alkaline water oxidation. Small, 2022, 18: 2204135
84 Zhang W, lv Q, Hou L, et al. Facile top-down fabrication of integrated amorphous NiFe-based electrocatalytic electrodes for high current and long-life oxygen evolution. J Mater Sci Tech, 2025, 211: 11–21
85 Li H, Wang Y, Liu C, et al. Enhanced OER performance of NiFeB amorphous alloys by surface self-reconstruction. Int J Hydrogen Energy, 2022, 47: 20718–20728
86 Xiao L, Liang Y, Li Z, et al. Amorphous FeNiNbPC nanoprous structure for efficient and stable electrochemical oxygen evolution. J Colloid Interface Sci, 2022, 608: 1973–1982
87 Zhou X, Zhu H, Fu S, et al. Atomic structure amorphization and electronic structure reconstruction of $FeCoNiCrMo_x$ high-entropy alloy nanoparticles for highly efficient water oxidation. Small, 2024, 20: 2405596
88 Chen H, Xin Y, Wu Y, et al. Boosting the activity and stability of self-supporting FeCoNiMoPB amorphous alloy for oxygen evolution. J Alloys Compd, 2023, 947: 169478
89 Xiao L, Gao J, Yao X, et al. Unraveling the role of nanocrystalline in amorphous nanoporous FeCoB catalysts for turning oxygen evolution activity and stability. Appl Surf Sci, 2023, 640: 158395
90 Jiang J, Guo X, Xin Y, et al. Architecting the metal-nonmetal oxide layers for boosting the oxygen-evolving intrinsic activity of amorphous alloy. Chem Eng J, 2024, 479: 147552
91 Chunduri A, Bhide A, Gupta S, et al. Exploring the role of multi-catalytic sites in an amorphous Co-W-B electrocatalyst for hydrogen and oxygen evolution reactions. ACS Appl Energy Mater, 2023, 6: 4630–4641
92 Jin Y, Xi G, Li R, et al. Nanoporous metallic-glass electrocatalysts for highly efficient oxygen evolution reaction. J Alloys Compd, 2021, 852: 156876
93 Wu K, Chu F, Meng Y, et al. Cathodic corrosion activated Fe-based nanoglass as a highly active and stable oxygen evolution catalyst for water splitting. J Mater Chem A, 2021, 9: 12152–12160
94 Li H, Zhu Z, Wang Y, et al. Disordered and oxygen vacancy-rich NiFe hydroxides/oxides *in situ* grown on amorphous ribbons for boosted alkaline water oxidation. J Electroanal Chem, 2021, 880: 114918
95 Aneeshkumar K S, Tseng J, Liu X, et al. Electrochemically dealloyed nanoporous $Fe_{40}Ni_{20}Co_{20}P_{15}C_5$ metallic glass for efficient and stable electrocatalytic hydrogen and oxygen generation. RSC Adv, 2021, 11: 7369–7380
96 Pang Y, Xu W, Zhu S, et al. Self-supporting amorphous nanoporous NiFeCoP electrocatalyst for efficient overall water splitting. J Mater Sci Tech, 2021, 82: 96–104
97 Wei R, Zhang K, Zhao P, et al. Defect-rich FeCoNiPB/$(FeCoNi)_3O_{4-x}$ high-entropy composite nanoparticles for oxygen evolution reaction: Impact of surface activation. Appl Surf Sci, 2021, 549: 149327
98 Jiang S, Zhu L, Yang Z, et al. Enhanced electrocatalytic performance of FeNiCoP amorphous alloys as oxygen-evolving catalysts for electrolytic water splitting application. Electrochim Acta, 2021, 368: 137618
99 Chen S Q, Li M, Ji Q, et al. Functional 3D nanoporous Fe-based alloy from metallic glass for high-efficiency water splitting and wastewater treatment. J Non-Cryst Solids, 2021, 571: 121070
100 Xi G, Zuo L, Li X, et al. *In-situ* constructed Ru-rich porous framework on NiFe-based ribbon for enhanced oxygen evolution reaction in alkaline solution. J Mater Sci Tech, 2021, 70: 197–204
101 Liu D, Song Z, Cheng S, et al. Mesoporous IrNiTa metal glass ribbon as a superior self-standing bifunctional catalyst for water electrolysis. Chem Eng J, 2022, 431: 134210
102 Wang H, Wei R, Li X, et al. Nanostructured amorphous $Fe_{29}Co_{27}Ni_{23}Si_9B_{12}$ high-entropy-alloy: An efficient electrocatalyst for oxygen evolution reaction. J Mater Sci Tech, 2021, 68: 191–198
103 Overa S, Crandall B S, Shrimant B, et al. Enhancing acetate selectivity by coupling anodic oxidation to carbon monoxide electroreduction. Nat

Catal, 2022, 5: 738–745
104 Cheng H, Dong B, Liu Q, et al. Direct electrocatalytic methanol oxidation on MoO_3/$Ni(OH)_2$: Exploiting synergetic effect of adjacent Mo and Ni. J Am Chem Soc, 2023, 145: 26858–26862
105 Zhang T, Sun Y, Li X, et al. PtPdAg hollow nanodendrites: Template-free synthesis and high electrocatalytic activity for methanol oxidation reaction. Small Methods, 2020, 4: 1900709
106 Qiu Y, Fan J, Wu J, et al. Atomically dispersed CrO_x on Pd metallene for CO-resistant methanol oxidation. Nano Lett, 2023, 23: 9555–9562
107 Baksi A, Nandam S H, Wang D, et al. $Ni_{60}Nb_{40}$ nanoglass for tunable magnetism and methanol oxidation. ACS Appl Nano Mater, 2020, 3: 7252–7259
108 Deng C, Toe C Y, Li X, et al. Earth-abundant metal-based electrocatalysts promoted anodic reaction in hybrid water electrolysis for efficient hydrogen production: Recent progress and perspectives. Adv Energy Mater, 2022, 12: 2201047
109 Ge J, Kuang J, Xiao Y, et al. Recent development of nickel-based catalysts and *in situ* characterization techniques for mechanism understanding of the urea oxidation reaction. Surfs Interfaces, 2023, 41: 103230
110 Song Y, Huang J, Tang C, et al. Improved urea oxidation performance via interface electron redistributions of the $NiFe(OH)_x$/MnO_2/NF p-p heterojunction. Small, 2024, 20: 2403612
111 Sohel A, Kovilakath M S N, Gogoi P J, et al. Mechanistic insights into the stabilization of *in situ* formed γ-NiOOH species on $Ni_{60}Nb_{40}$ nanoglass for effective urea electro-oxidation. Small, 2024, 20: 2405160
112 Sarkar S, Ponce N T, Banerjee A, et al. Green polymeric nanomaterials for the photocatalytic degradation of dyes: A review. Environ Chem Lett, 2020, 18: 1569–1580
113 Wang W M, Li X, Du X, et al. A feasible approach for azo dye degradation using natural magnetite in heterogeneous fenton oxidation. Water Cycle, 2022, 3: 100–105
114 Shanker U, Rani M, Jassal V. Degradation of hazardous organic dyes in water by nanomaterials. Environ Chem Lett, 2017, 15: 623–642
115 Zhang L, Qiu L, Zhu Q, et al. Insight into efficient degradation of 3,5-dichlorosalicylic acid by Fe-Si-B amorphous ribbon under neutral condition. Appl Catal B-Environ, 2021, 294: 120258
116 Crane R A, Scott T B. Nanoscale zero-valent iron: Future prospects for an emerging water treatment technology. J Hazard Mater, 2012, 211-212: 112–125
117 Miao F, Wang Q, Zeng Q, et al. Excellent reusability of FeBC amorphous ribbons induced by progressive formation of through-pore structure during acid orange 7 degradation. J Mater Sci Tech, 2020, 38: 107–118
118 Peng X, Han J, Wang Y, et al. Unexpected enhanced catalytic performance via highly dense interfaces in ultra-fine amorphous-nanocrystalline biphasic structure. Appl Mater Today, 2022, 29: 101689

Application of amorphous alloys in catalysis

WU Yong & YU Peng*

College of Physics and Electronic Engineering, Chongqing Normal University, Chongqing 401331, China
**Corresponding author (email: pengyu@cqnu.edu.cn)*

With economic and population growth, the global demand for energy and the pressure on the environment are rapidly increasing. The over-exploitation and consumption of fossil energy sources have led to a series of problems (such as energy depletion, environmental pollution, and global warming) that seriously endanger the survival and development of humankind. Reducing the utilization of fossil energy sources is the key to achieving carbon neutrality and peak carbon goals. A viable strategy is the development of catalysis, which can produce and store clean, sustainable energy. Different catalytic processes produce sustainable energy sources depending on different reaction mechanisms, but their realization and eventual commercialization rely on the development of high-performance catalysts. Amorphous alloys exhibit a series of excellent mechanical, physical, and chemical properties due to their unique disordered microstructure. Amorphous alloys, as new and efficient catalysts, have a wide range of applications in the field of energy storage and conversion. Compared with crystalline materials, they have the following advantages. (1) Amorphous alloys can adjust their compositional structure within a wide range. (2) Amorphous alloys are isotropic, do not have defects such as grain boundaries and segregation, and have uniform active sites as well as corrosion resistance. (3) Amorphous alloys can be prepared under flexible conditions. (4) Amorphous alloys have a high surface energy as well as a high degree of unsaturated coordination, which enables some chemical reactants and intermediates to be adsorbed on specific sites in an appropriate form. (5) Amorphous alloys have a metastable structure, which is prone to surface reconstruction under extreme physical or chemical conditions, changing from inert species to active-phase species. Amorphous alloys, with their unique structure and performance advantages, make them a catalytic material with great application prospects. This article briefly summarizes the research progress, performance advantages, and application potential of amorphous alloy catalysts. Furthermore, the challenges of amorphous alloy catalysts and their prospects are also summarized.

amorphous alloys, catalysts, performance advantages, application prospects

PACS: 61.43.Er, 71.55.Jv, 78.55.Qr, 82.47.-a, 84.60.-h

doi: 10.1360/SSPMA-2024-0410